Hydrogen Storage

DOI: 10.1002/ange.200601991

High H_2 Adsorption by Coordination-Framework Materials**

Xiang Lin, Junhua Jia, Xuebo Zhao, K. Mark Thomas, Alexander J. Blake, Gavin S. Walker, Neil R. Champness, Peter Hubberstey,* and Martin Schröder**

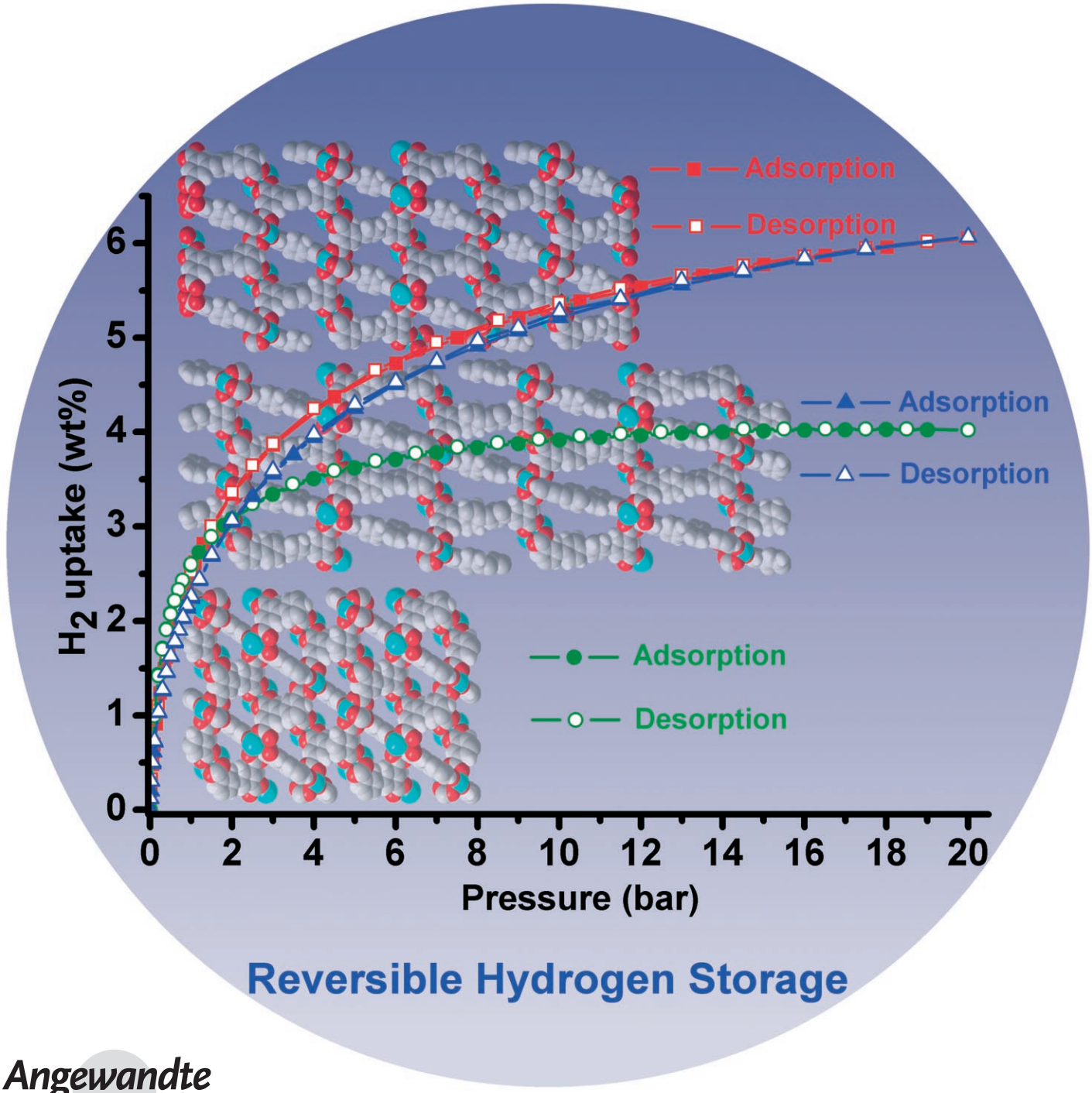

The storage of H_2 in a safe and compact form represents a significant current challenge,[1] and there is wide-ranging interest in materials that can store and release H_2 with fast kinetics and high reversibility over multiple cycles.[2] Porous coordination frameworks have become competitors to other porous materials, such as zeolites[3] and carbon materials (for example, activated carbon or nanotubes),[4] with recent studies confirming that these frameworks can store considerable quantities of H_2 at 78 K.[5–11] Most studies of H_2 adsorption in coordination frameworks focus on the low-pressure region (0–1 bar) and, therefore, do not fully address the relationship between porosity and storage capacity. Although recent high-pressure volumetric measurements on some coordination frameworks revealed a correlation between maximum uptake and surface area,[9] the study involved several coordination frameworks with different structure types, and the influence of pore size and shape on guest adsorption was not investigated systematically. Herein, we report the structures of three close structural analogues, along with studies of high-pressure H_2 adsorption by these materials, to establish a route to higher H_2 storage capacity.

In coordination frameworks, the metal cations and carboxylate ligands can form a range of multinuclear nodes with predefined geometries (for example, the binuclear paddle-wheel units $\{Zn_2(O_2CR)_4\}$[12] and $\{Cu_2(O_2CR)_4\}$[5,10,13] (4-connected), the trinuclear units $\{Ni_3O(O_2CR)_6\}$, $\{Fe_3O(O_2CR)_6\}$,[6,14] and $\{Cr_3O(O_2CR)_6\}$[11] (6-connected), and the tetranuclear unit $\{Zn_4O(O_2CR)_6\}$[7,15] (6-connected)), which are largely dependent upon the metal cation and the reaction stoichiometry. The three coordination-framework materials in this study are based on biphenyl, terphenyl, and quaterphenyl tetracarboxylic acids. By varying the length of the organic backbone of these ligands, we obtain the desired structural analogues, in terms of framework composition and topology, and thereby investigate the correlation of pore size with gas-adsorption behavior.

Biphenyl-3,3′,5,5′-tetracarboxylic acid (H_4L^1; Figure 1) was synthesized by the oxidation of 3,3′,5,5′-tetramethylbiphenyl with $KMnO_4$. Terphenyl-3,3″,5,5″-tetracarboxylic acid (H_4L^2; Figure 1) and quaterphenyl-3,3‴,5,5‴-tetracarboxylic acid (H_4L^3; Figure 1) were synthesized by the Suzuki coupling of diethylisophthalate-5-boronic acid and dibromobenzene (for H_4L^2) or dibromobiphenyl (for H_4L^3). Solvothermal reaction of H_4L^1, H_4L^2, or H_4L^3 with $Cu(NO_3)_2{\cdot}2.5\,H_2O$ in a slightly acidified mixture of DMF/1,4-dioxane/H_2O afforded the solvated framework compounds $[Cu_2(L^1)(H_2O)_2]$ (**1**), $[Cu_2(L^2)(H_2O)_2]$ (**2**), and $[Cu_2(L^3)(H_2O)_2]$ (**3**), respectively (Figure 1). Acidic reaction solutions are necessary to obtain crystalline products; aqueous HCl is the most effective acid for this purpose. We were unable to reproduce the preparation of **1** in pure crystalline form by following the reported procedure,[5] but with our experimental procedures, the complex can be synthesized in good yield, in a highly crystalline form.

Crystal-structure determinations for **1**–**3** confirm that all three compounds have the same framework topology. Each Cu^{II} ion is coordinated by five O atoms in a square pyramidal geometry. Pairs of Cu^{II} centers are bridged by four carboxylate groups, forming $\{Cu_2(O_2CR)_4\}$ paddle-wheel units (Figure 2). One H_2O molecule binds to each metal centre along the paddle-wheel axis. Each $\{Cu_2(O_2CR)_4\}$ paddle wheel is linked to four biphenyl, terphenyl, or quaterphenyl connectors (and vice versa; Figure 2), to give frameworks with NbO-type topologies.

Views of the structures of **1**–**3** along the *c* axes reveal hexagonal channels that run through the frameworks (Figure 1). The diameters of the channels are predefined by the geometry of the $\{Cu_2(O_2CR)_4\}$ units and the span of the dicarboxylato moieties of the isophthalate groups on each terminus of the bridging ligands. Therefore, the diameters of the channels are the same in all three structures, approximately 5.0 Å. These channels are interconnected through triangular windows, which can be seen in views of the structures along the *a* or *b* axes (Figure 1). Because of the variation in ligand length, the size of the triangular windows expands on going from **1**–**3**. While it is difficult to derive reliable estimates of pore size from the crystal structures, pore size distributions (PSDs) derived from the N_2 isotherms of the desolvated materials at 78 K suggest that the pore size increases from **1**–**3** (Table 1). The solvent molecules in the as-prepared crystals are disordered within the pores; their contributions to the X-ray diffraction patterns were estimated by using PLATON/SQUEEZE.[16] By using PLATON/SOLV,[16] the accessible voids in the desolvated structures of **1**, **2**, and **3** were estimated to correspond to 63.3, 70.4, and 75.5 % of the total volumes, respectively (Table 1). Powder X-ray diffraction (PXRD) was used to confirm the phase purity and to examine the crystallinity of bulk samples. Thermal gravimetric analysis (TGA) was used to verify the ratio of Cu/L in the desolvated compounds (see Supporting Information).

The free solvent molecules in the Cu^{II} complexes can be readily exchanged for other organic solvents (for example, acetone) or removed by heating at 100 °C, either under a flow

[*] Dr. X. Lin, J. Jia, Dr. A. J. Blake, Prof. Dr. N. R. Champness, Dr. P. Hubberstey, Prof. Dr. M. Schröder
School of Chemistry
University of Nottingham
University Park, NG72RD (UK)
Fax: (+44) 115-951-3563
E-mail: Neil.Champness@nottingham.ac.uk
Peter.Hubberstey@nottingham.ac.uk
m.schroder@nottingham.ac.uk

Dr. G. S. Walker
School of Mechanical Materials & Manufacturing Engineering
University of Nottingham
University Park, NG72RD (UK)

Dr. X. B. Zhao, Prof. Dr. K. M. Thomas
Northern Carbon Research Laboratories
Department of Chemistry
University of Newcastle upon Tyne
Newcastle upon Tyne, NE1 7RU (UK)

[**] We thank the EPSRC (UKSHEC) for support, and the CVCP and the University of Nottingham for funding (to J.J.). M.S. gratefully acknowledges the receipt of a Royal Society Wolfson Merit Award and a Royal Society Leverhulme Trust Senior Research Fellowship.

Supporting information for this article is available on the WWW under http://www.angewandte.org or from the author.

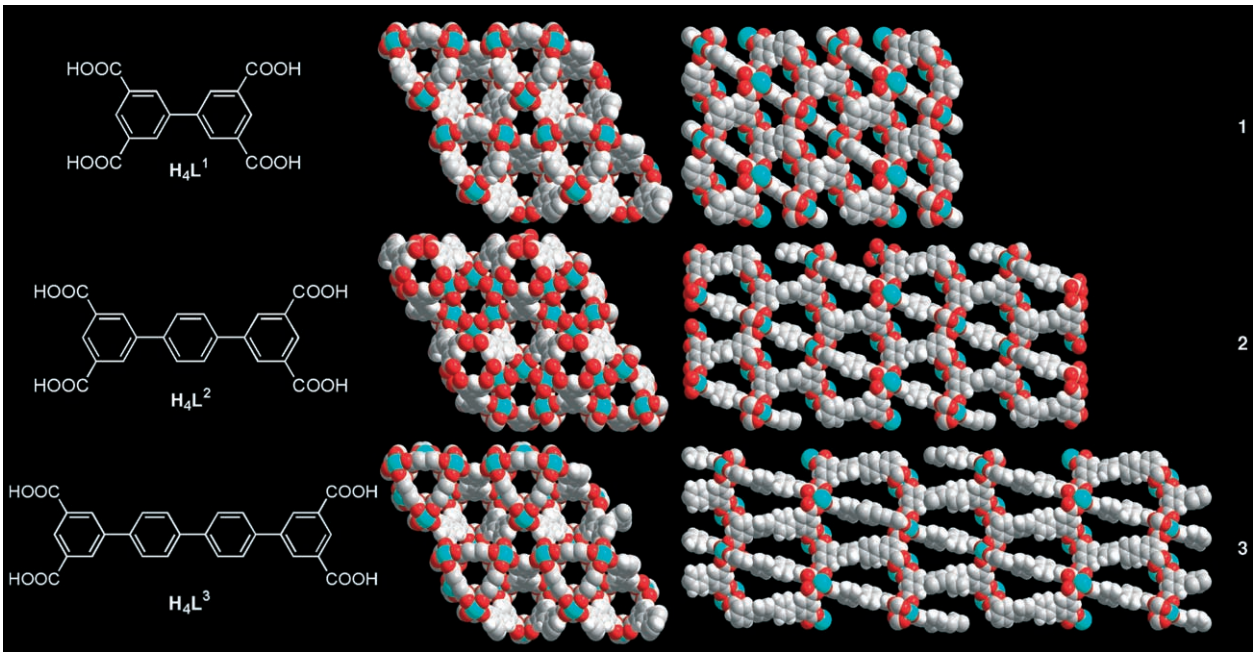

Figure 1. Acidic forms H_4L^1, H_4L^2, and H_4L^3 (left) of the ligands in **1**–**3**. Space-filling representations of **1**–**3** viewed along the *c* axes (middle) and along the *a* axes (right) of the structures; Cu blue, C gray, H white, O red; disordered solvent molecules omitted.

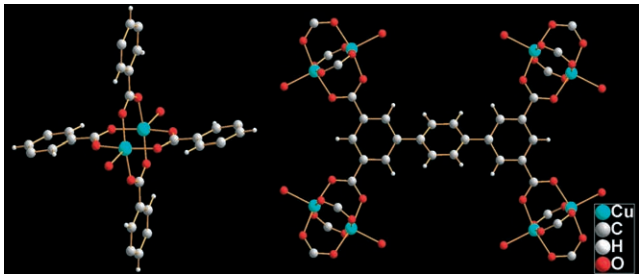

Figure 2. The 4-connected $\{Cu_2(O_2CR)_4\}$ paddle-wheel unit (left) and the 4-connected L^2 ligand (right) of **2**.

of N_2 gas or under vacuum. Compounds **1**–**3** show very similar thermal behavior, as determined by TGA. The as-synthesized blue-green crystalline samples lose solvent rapidly over 25–120 °C, resulting in a deep purple-blue crystalline material. A plateau is observed from 120–300 °C in the TGA profiles, indicating no further weight loss, and above 300 °C the complexes start to decompose rapidly to produce CuO. The desolvated samples of **1**–**3** are stable in a dry environment, and the structural integrity of the framework is retained in each case, as verified by PXRD. However, once in contact with moisture, their color rapidly reverts to blue-green, and the samples lose crystallinity and porosity.

To study the sorption isotherms of the evacuated frameworks, the acetone-exchanged samples were degassed at 100 °C and 10^{-10} bar for 16 h to give fully desolvated **1**–**3**. The isotherms for N_2, H_2, and D_2 sorption were measured at 78 K.

The N_2 sorption isotherms for **1**–**3** show typical type-I adsorption behavior, confirming the retention of the microporous structures after the removal of solvent from the crystalline samples (Figure 3a). The BET surface areas for desolvated **1**–**3** were estimated as 1670, 2247, and 2932 $m^2 g^{-1}$, respectively (Table 1). These high surface areas do not represent "true" surface areas, since there are contributions from pore-filling effects. However, BET surface areas do give an indication of the adsorption capacities of porous materials.[17] The pore sizes determined by applying a Dubinin–Astakhov analysis to the sorption data are narrowly distributed around 6.5, 7.3, and 8.3 Å for desolvated **1**, **2**, and **3**, respectively (Table 1). The pore volumes calculated from the maximum amount of N_2 adsorbed are 0.680, 0.886, and 1.138 $cm^3 g^{-1}$ for desolvated **1**, **2** and **3**, respectively (Table 1). These data clearly show that using longer ligands can produce more porous materials with higher adsorption capacities.

Table 1: Physical characteristics and sorption properties of **1**–**3**.

	N_2 uptake (1 bar) [$cm^3 g^{-1}$]	BET area [$m^2 g^{-1}$]	Calcd density[a] [$g cm^{-3}$]	Expt density[b] [$g cm^{-3}$]	Accessible voids[a] [%]	Pore volume[a] [$cm^3 g^{-1}$]	Pore volume (N_2)[c] [$cm^3 g^{-1}$]	Pore size (N_2)[c] [Å]	H_2 uptake (1/20 bar) [wt%]	Max H_2 uptake[d] [wt%]	Adsorbed H_2 density (20 bar/max) [$g cm^{-3}$]	Max H_2 uptake [$g L^{-1}$]
1	448	1670	0.927	1.75	63.3	0.683	0.680	6.5	2.59/4.02	4.20	0.0591/0.0615	38.9
2	573	2247	0.650	1.67	70.4	1.083	0.886	7.3	2.52/6.06	6.70	0.0560/0.0619	43.6
3	736	2932	0.587	1.60	75.5	1.284	1.138	8.3	2.24/6.07	7.01	0.0472/0.0546	41.1

[a] Calculated using PLATON/SOLV;[16] [b] determined from He sorption isotherms at 273 K; [c] determined from N_2 sorption isotherms at 78 K; [d] determined from Langmuir plots.

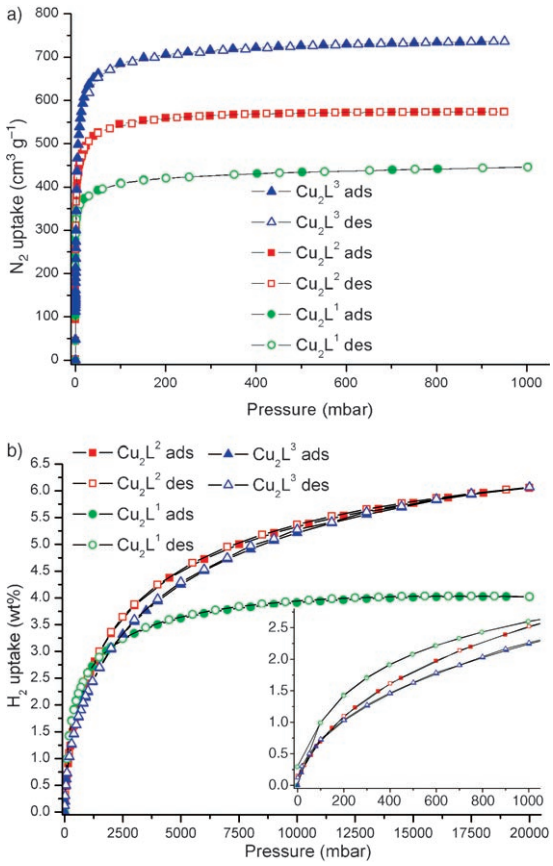

Figure 3. a) N_2 and b) H_2 sorption isotherms measured for desolvated **1**–**3** at 78 K; the inset in (b) is an enlargement of the low-pressure region of the H_2 isotherms; ads = adsorption, des = desorption

Gravimetric H_2 sorption isotherms were recorded from 0–20 bar at 78 K (Figure 3b). All data were rigorously corrected for the buoyancy of the system, samples, and adsorbates. The sample densities used in the buoyancy corrections were determined from He displacement isotherms (up to 20 bar) measured at 273 K. The H_2 sorption isotherms of desolvated **1**–**3** show good reversibility and an absence of hysteresis. Kinetic data for H_2 adsorption confirm that equilibrium is achieved rapidly, within approximately 3 min of an isotherm pressure step. These data are consistent with typical H_2 adsorption and exclude any significant effects due to the presence of impurities. Importantly, D_2 sorption isotherms were measured to verify that the observed H_2 adsorption is due to H_2, rather than other impurities (see Supporting Information). We obtained values of 1.05–1.20 for the molar ratio of adsorbed D_2/H_2 over 0.1–9.0 bar at 78 K, which are comparable to the values obtained for porous carbon materials at 78 K (1.06–1.10);[18,19] values of approximately 1.16 have been observed for zeolite NaA.[20]

The H_2 sorption isotherm of desolvated **1** reveals an uptake of 2.59 wt% at 1 bar, which is slightly higher than the reported value (2.47 wt%), although the BET surface area of desolvated **1** determined from the N_2 sorption isotherm is lower than the reported value.[5] Desolvated **2** adsorbs 2.52 wt% H_2 at 1 bar. This uptake is similar to that observed for **1**, but in the low-pressure region (0–800 mbar), the H_2 adsorption of **2** is significantly lower than that of **1**. Desolvated **3** has the lowest H_2 adsorption at 1 bar, 2.24 wt%, despite having the largest pore size. At low H_2 pressures, the H_2 adsorption is still far from saturation for desolvated **1**–**3**, indicating that their H_2 storage capacity is dominated by the affinity between H_2 molecules and the frameworks. Given that **1**–**3** all have the same NbO topology and have chemically very similar internal surfaces comprising binuclear Cu–carboxylate nodes and aryl groups, the implication of our adsorption results is that a smaller pore size leads to a higher affinity for H_2 adsorption. Interestingly, the frameworks of **1**–**3**, which contain binuclear Cu nodes, show significantly higher H_2 uptakes than related frameworks based on Zn or Fe nodes.[6,7,14,15]

When the H_2 pressure is increased, desolvated **1** adsorbs additional H_2 gas, until saturation is nearly reached at 10 bar; above this pressure, **1** has very little potential to adsorb more H_2. The highest adsorption of H_2 by **1**, 4.02 wt%, was recorded at 20 bar. The adsorption data above 2 bar can be fitted to the Langmuir equation, from which a maximum adsorption of 4.20 wt% is predicted for **1** (Table 1). Compound **2** incorporates a longer organic ligand than **1**, resulting in a larger pore volume and, correspondingly, a higher surface area. Thus, **2** has a greater potential for H_2 adsorption at higher pressures. At 1.2 bar, the adsorption of H_2 by **2** begins to exceed that observed for **1**, and at 20 bar, **2** adsorbs a remarkable 6.06 wt% of H_2. Thus, although **1** has the highest affinity for H_2, its small pore volume imposes an upper limit on its absorption of the gas.

Compound **3** incorporates the longest organic ligand and has the largest pore volume and surface area of the three compounds. Although it has the lowest uptake at 1 bar, 2.24 wt%, it also shows good potential to store H_2. At 2.5 bar, its uptake exceeds that observed for **1**, and at 20 bar, it has an uptake of 6.07 wt% H_2, which is comparable to that observed for **2**. It can be anticipated that higher H_2 adsorption would be observed at pressures higher than 20 bar. Fitting the high-pressure region of the H_2 isotherms of **2** and **3** to the Langmuir equation gives maximum adsorptions of 6.70 wt% and 7.01 wt% H_2, respectively (Table 1).

The three compounds not only have excellent gravimetric H_2 storage capacities, but also have volumetric storage capacities that are the highest yet reported for coordination frameworks (Table 1). Significantly, the value of 43.6 $g\,L^{-1}$ observed for **2** is very close to the 2010 U.S. Department of Energy (DOE) target of 45 $g\,L^{-1}$.[21] The data in Table 1 indicate that the crystallographic pore volume has the closest correlation with the maximum theoretical H_2 uptake for **1** and **2**. Thus, for desolvated **1**–**3**, the ratios of the crystallographic pore volumes are 1:1.59:1.88, respectively, and the ratios for the N_2 pore volumes are 1:1.30:1.67, respectively. The maximum theoretical H_2 uptake obtained from Langmuir isotherms for **1**–**3** are 1:1.60:1.67, respectively (Table 1). From **1** to **2**, the proportional increase in the maximum possible H_2 uptake is larger than that in pore volume, presumably because of a more optimal pore geometry in **2**. However, the proportional increase in the maximum H_2 uptake from **2** to **3** is less than that in pore volume, reflecting the comparatively lower affinity between H_2 molecules and the pores of **3**.

Given that the density of liquid H_2 is 0.0708 g cm^{-3} at 20 K,[22] the densities for adsorbed H_2 calculated herein (Table 1) suggest that H_2 is highly compressed within the pores of **1**–**3**. The densities are similar to the values reported for H_2 adsorption on porous carbon materials (0.05–0.06 g cm^{-3}).[19] However, the carbon materials have a large PSD, whereas in crystalline metal–organic frameworks, the pores sizes are generally well-defined. The H_2 uptake and adsorbed H_2 density under low-pressure conditions decrease with increasing pore size from **1**–**3** (determined by ligand length), while the maximum amount of H_2 adsorbed increases while the maximum adsorbate density decreases with increasing pore size. These effects are related to the enhancement of adsorption in smaller pores at low pressures due to the overlap of the potential energy fields of the pore walls. The contrasting trends of increasing maximum H_2 uptake and decreasing adsorbed H_2 density with increasing pore size suggest that an optimum pore size exists. Therefore, a strategy of only increasing pore volume may not give the optimum material.

Férey and co-workers have synthesized $[Cr_3F(H_2O)_2(bdc)_3]\cdot n\,H_2O$ ($n \approx 25$; bdc = benzene-1,4-dicarboxylate), which has a cubic zeotype structure with a very large cell volume (ca. 702 000 Å^3) and containing a hierarchy of large pores.[23] The material has an N_2 pore volume of 2.0(1) cm^3 g^{-1} and a Langmuir surface area of approximately 5900 m^2 g^{-1}. Interestingly, H_2 adsorption studies on this material demonstrated that it adsorbs 4.5 wt % H_2 at 77 K and 3 MPa, with the density of the adsorbed H_2 being lower than in **1**–**3**. However, higher-pressure data are required to identify the maximum density of adsorbed H_2 for this material. Also, one could argue that the maximum possible density of H_2 within a porous framework is that of solid H_2, which is 0.077 g cm^{-3} at the triple point (13.8 K).[22] This density might be more appropriate for comparison with the densities of H_2 adsorbed at very low temperatures, while the liquid density is probably a better model for experiments at 78 K.

In summary, the sorption isotherms for desolvated **1**–**3** do not provide any evidence of adsorption of H_2 on different types of sites within the frameworks, but confirm that H_2 adsorption is controlled by the available pore volume, with a proportional decrease in adsorbate density with increasing pore size (Table 1). The adsorption of supercritical H_2 is limited by its low interaction energy with adsorbent surfaces, and this interaction potential can be enhanced in nanosized pores by overlap of the potential fields from both sides of the pore.[24] There is, thus, an intrinsic conflict between the large pore volume required to enhance H_2 storage capacity and the resulting decrease in the strength of the interaction in larger pores. Open metal centers are potentially significant, in that they are part of the porous structure, but have the disadvantage that they will adsorb H_2 impurities, such as H_2O. The sorption isotherms of **1**–**3** are reversible, and there is no evidence for chemisorption of H_2. There are also no steps in the isotherms that might be indicative of either adsorption on different sites or, alternatively, structural changes in the flexible framework during adsorption. We conclude that increasing the pore volume is not the only factor to be considered in the design of H_2-storage materials, because the adsorbed H_2 density may decrease with increasing pore size, as demonstrated by the series of compounds reported herein (Table 1).

Given that four coordination frameworks (**2**, **3**, MOF-177,[9] and IRMOF-20[9]) have now achieved (at 78 K and pressures below 80 bar) the 6 wt % H_2 gravimetric storage capacity of the 2010 DOE guidelines,[21] and that the volumetric capacity of **2** is also very close to the 2010 DOE target of 45 g L^{-1}, it is reasonable to anticipate the discovery of new materials with enhanced H_2 storage. We are currently investigating the challenge of synthesizing new coordination frameworks for higher H_2 storage capacity by searching for new metal building blocks, by determining the optimum compromise between large total pore volume and small pore size, and by optimizing the framework topology for H_2 adsorption.

Experimental Section

H_4L^2 and H_4L^3: The ligands H_4L^2 and H_4L^3 were synthesized using similar experimental procedures. The synthesis of H_4L^2 is described herein. Dibromobenzene (0.234 g, 1 mmol), diethylisophthalate-5-boronic acid (0.64 g, 2.4 mmol), and K_3PO_4 (2.10 g, 10 mmol) were mixed in 1,4-dioxane (30 mL), and the mixture was de-aerated using N_2. $Pd(PPh_3)_4$ (0.05 g, 0.043 mmol) was added to the stirred reaction mixture, and the mixture was then heated at 80 °C for 3 days under an N_2 atmosphere. The resultant mixture was evaporated to dryness, extracted into $CHCl_3$, and then dried over $MgSO_4$. The solution was evaporated to dryness, and the residue was briefly washed with EtOH (10 mL). The resulting crude product (mainly tetraethyl esters of the target ligand) was hydrolyzed by heating in aqueous NaOH (2 M) under reflux, followed by acidification with aqueous HCl (37 %), affording H_4L^2 (yield: 0.28 g, 65 %). ^{1}H NMR ([D$_6$]DMSO, 300 MHz): H_4L^2: $\delta = 8.48$ (t, $J = 1.6$ Hz, 1H), 8.44 (d, $J = 2.1$ Hz, 2H), 7.91 ppm (s, 2H); H_4L^3: 8.48 (t, 1H), 8.45 (d, $J = 1.5$ Hz, 2H), 7.90 ppm (dd, $J = 1.1$ Hz 4H). Elemental analysis (%) calcd for H_4L^2 ($C_{22}O_8H_{14}$): C 65.03, H 3.47; found: C 64.87, H 3.59; calcd for H_4L^3 ($C_{28}O_8H_{18}$): C 69.71, H 3.76; found: C 69.59, H 3.90.

1–**3**: The same experimental procedure was employed in the syntheses of **1**–**3**. The synthesis of **2** is described herein. H_4L^2 (0.05 g, 0.12 mmol) and $Cu(NO_3)_2\cdot 2.5\,H_2O$ (0.1 g, 0.43 mmol) were mixed and dispersed in DMF/1,4-dioxane/H_2O (2:1:1 v/v/v, 15 mL). The resulting blue-green slurry turned clear upon addition of 2 drops of aqueous HCl (37 %). The solution was gradually heated to 80 °C over a period of 12 h, and kept at this temperature for 3 days. The blue crystalline product was separated by filtration when the solution was still warm (50 °C), washed sequentially by DMF/H_2O (1:2 v/v) and DMF, and then dried briefly in air (yield: 0.082 g, 75.8 %). Elemental analysis (%) calcd for **2** ($C_{36.50}H_{46.5}Cu_2N_{1.5}O_{17.5}$): C 47.99, H 5.13, N 2.30; found C 48.52, H 5.03, N 2.07; calcd for **3** ($C_{42.5}H_{54.5}Cu_2N_{1.5}O_{19.5}$): C 49.78, H 5.36, N 2.05; found C 49.60, H 4.56, N 1.58. The volatility of the co-crystallized solvents in the samples contributes to the discrepancy in the elemental analyses. The weight ratio of $[Cu_2(L)]/2\,CuO$ for desolvated samples ($[Cu_2(L)]$) was determined by TGA: calcd for **1**: 2.8365; found: 2.7630; calcd for **2**: 3.4528; found: 3.4760; calcd for **3**: 3.9308; found: 3.7299. IR (KBr): for **2**: $\tilde{\nu} = 1736$ (m), 1618 (vs), 1566 (vs), 1451 (s), 1406 (vs), 1384 (vs), 1303 (m), 1261 (m), 1111 (w), 1080 (w), 838 (m), 772 (m), 729 cm^{-1} (m); for **3**: $\tilde{\nu} = 1716$ (m), 1616 (s), 1558 (s), 1505 (s), 1442 (s), 1384 (vs), 1261 (w), 1020 (w), 824 (w), 767 (m), 730 (m), 669 (m), 630 cm^{-1} (w).

Crystal-structure determinations: intensity data for **2** and **3** were collected at 150(2) K on a Bruker SMART APEX CCD area-detector diffractometer using graphite-monochromated $Mo_{K\alpha}$ radiation. The structures were solved by direct methods and subsequent difference Fourier syntheses, and refined using the SHELXTL software package. The H atoms on the ligands were placed in idealized positions and refined using a riding model. The H atoms of the coordinated H_2O

molecules could not be located, but are included in the formulae. The unit cell includes a large region of disordered solvent molecules, which could not be modeled as discrete atomic sites. We employed PLATON/SQUEEZE[16] to calculate the diffraction contribution of the solvent molecules and, thereby, to produce a set of solvent-free diffraction intensities. The final formulae were calculated from the SQUEEZE results combined with the elemental analyses. **2**: $[Cu_2(C_{22}H_{10}O_8)(H_2O)_2]\cdot 1.5(C_3H_7NO)\cdot 2.5(C_4H_8O_2)\cdot H_2O$, $M_r = 913.3$, blue-green block, $0.07 \times 0.24 \times 0.26$ mm, trigonal, $R\bar{3}m$, $a = 18.629(1)$, $c = 38.492(2)$ Å, $V = 11569(2)$ Å^3, $Z = 9$, $\rho_{calcd} = 1.180$ g cm^{-3}, $\mu = 0.887$ mm^{-1}, $F(000) = 4266$, 23387 reflections, 3244 unique, $R_{int} = 0.055$, $R_1 = 0.0353$, $wR_2 = 0.0947$, GOF = 0.949, max/min residual electron density = 0.72/−0.24 e Å^{-3}. **3**: $[Cu_2(C_{28}H_8O_{14})(H_2O)_2]\cdot 1.5(C_3H_7NO)\cdot 2.5(C_4H_8O_2)\cdot 3H_2O$, $M_r = 1025.5$, blue-green block, $0.14 \times 0.15 \times 0.40$ mm, trigonal, $R\bar{3}m$, $a = 18.434(1)$, $c = 52.364(3)$ Å, $V = 15409(2)$ Å^3, $Z = 9$, $\rho_{calcd} = 0.995$ g cm^{-3}, $\mu = 0.674$ mm^{-1}, $F(000) = 4806$, 93972 reflections, 4319 unique, $R_{int} = 0.051$, $R_1 = 0.0393$, $wR_2 = 0.1073$, GOF = 0.871, max/min residual electron density = 0.45/−0.25 e Å^{-3}. CCDC-606908 (**2**) and CCDC-606909 (**3**) contain the supplementary crystallographic data for this paper. These data can be obtained free of charge from The Cambridge Crystallographic Data Centre via www.ccdc.cam.ac.uk/data_request/cif.

Sorption isotherms: N_2, H_2, and D_2 sorption isotherms were measured using a Hiden Isochema Intelligent Gravimetric Analyser (IGA-003), which is an ultra-high-vacuum, clean instrument with a diaphragm and turbo pumping system. H_2 and D_2 were purified by using calcium aluminosilicate and activated carbon adsorbents to remove trace amounts of H_2O and other impurities. The measurement protocols used were validated by the complete desorption of H_2 and the comparison of results from porous carbon samples on two different instruments.

The Supporting Information includes additional views of the crystal structures, PXRD patterns, TGA profiles, PSD analyses, detailed H_2 and D_2 sorption isotherms, Langmuir fitting analyses, and further experimental details.

Received: May 18, 2006
Revised: June 23, 2006
Published online: August 23, 2006

Keywords: adsorption · copper · hydrogen storage · metal–organic frameworks · microporous materials

[1] L. Schlapbach, *MRS Bull.* **2002**, *27*, 675 – 676.
[2] M. G. Nijkamp, J. E. M. J. Raaymakers, A. J. van Dillen, K. P. de Jong, *Appl. Phys. A* **2001**, *72*, 619 – 623.
[3] H. W. Langmi, A. Walton, M. M. Al-Mamouri, S. R. Johnson, D. Book, J. D. Speight, P. P. Edwards, I. Gameson, P. A. Anderson, I. R. Harris, *J. Alloys Compd.* **2003**, *356–357*, 710 – 715; A. Zecchina, S. Bordiga, J. G. Vitillo, G. Ricchiardi, C. Lamberti, G. Spoto, M. Bjorgen, K. P. Lillerud, *J. Am. Chem. Soc.* **2005**, *127*, 6361 – 6366; J. Eckert, J. M. Nicol, J. Howard, F. R. Trouw, *J. Phys. Chem.* **1996**, *100*, 10646 – 10651.
[4] B. Panella, M. Hirscher, S. Roth, *Carbon* **2005**, *43*, 2209 – 2214; H. G. Schimmel, G. J. Kearley, M. G. Nijkamp, C. T. Visser, K. P. de Jong, F. M. Mulder, *Chem. Eur. J.* **2003**, *9*, 4764 – 4770; G. Gundiah, A. Govindaraj, N. Rajalakshmi, K. S. Dhathathreyan, C. N. R. Rao, *J. Mater. Chem.* **2003**, *13*, 209 – 213; M. Becher, M. Haluska, M. Hirscher, A. Quintel, V. Skakalova, U. Dettlaff-Weglikovska, X. Chen, M. Hulman, Y. Choi, S. Roth, V. Meregalli, M. Parrinello, R. Strobel, L. Jorissen, M. M. Kappes, J. Fink, A. Zuttel, I. Stepanek, P. Bernier, *C. R. Phys.* **2003**, *4*, 1055 – 1062; A. Zuttel, P. Sudan, P. Mauron, T. Kiyobayashi, C. Emmenegger, L. Schlapbach, *Int. J. Hydrogen Energy* **2001**, *26*, 203 – 212; M. S. Dresselhaus, K. A. Williams, P. C. Eklund, *MRS Bull.* **1999**, *24*, 45 – 50; M. Rzepka, P. Lamp, M. A. de la Casa-Lillo, *J. Phys. Chem. B* **1998**, *102*, 10894 – 10898; A. C. Dillon, K. M. Jones, T. A. Bekkedahl, C. H. Kiang, D. S. Bethune, M. J. Heben, *Nature* **1997**, *386*, 377 – 379; Y. Gogotsi, R. K. Dash, G. Yushin, T. Yildirim, G. Laudisio, J. E. Fischer, *J. Am. Chem. Soc.* **2005**, *127*, 16006 – 16007.
[5] B. Chen, N. W. Ockwig, A. R. Millward, D. S. Contreras, O. M. Yaghi, *Angew. Chem.* **2005**, *117*, 4823 – 4827; *Angew. Chem. Int. Ed.* **2005**, *44*, 4745 – 4749. $[Cu_2(L^1)(H_2O)_2]$ (**1**) has also been termed MOF-505.
[6] A. C. Sudik, A. R. Millward, N. W. Ockwig, A. P. Côté, J. Kim, O. M. Yaghi, *J. Am. Chem. Soc.* **2005**, *127*, 7110 – 7118.
[7] J. L. C. Rowsell, A. R. Millward, K. S. Park, O. M. Yaghi, *J. Am. Chem. Soc.* **2004**, *126*, 5666 – 5667.
[8] N. L. Rosi, J. Eckert, M. Eddaoudi, D. T. Vodak, J. Kim, M. O'Keeffe, O. M. Yaghi, *Science* **2003**, *300*, 1127 – 1130; J. L. C. Rowsell, J. Eckert, O. M. Yaghi, *J. Am. Chem. Soc.* **2005**, *127*, 14904 – 14910; S. S. Kaye, J. R. Long, *J. Am. Chem. Soc.* **2005**, *127*, 6506 – 6507; J. L. C. Rowsell, O. M. Yaghi, *J. Am. Chem. Soc.* **2006**, *128*, 1304 – 1315; B. Kesanli, Y. Cui, M. R. Smith, E. W. Bittner, B. C. Brockrath, W. Lin, *Angew. Chem.* **2005**, *117*, 74 – 77; *Angew. Chem. Int. Ed.* **2005**, *44*, 72 – 75.
[9] A. G. Wong-Foy, A. J. Matzger, O. M. Yaghi, *J. Am. Chem. Soc.* **2006**, *128*, 3494 – 3495.
[10] D. Sun, S. Ma, Y. Ke, D. J. Collins, H.-C. Zhou, *J. Am. Chem. Soc.* **2006**, *128*, 3896 – 3897.
[11] A. Vimont, J. M. Goupil, J. C. Lavalley, M. Daturi, S. Surblé, C. Serre, F. Millange, G. Férey, N. Audebrand, *J. Am. Chem. Soc.* **2006**, *128*, 3218 – 3227; S. Surblé, C. Serre, C. Mellot-Draznieks, F. Millange, G. Férey, *Chem. Commun.* **2006**, 284 – 286.
[12] M. E. Braun, C. D. Steffek, J. Kim, P. G. Rasmussen, O. M. Yaghi, *Chem. Commun.* **2001**, 2532 – 2533; M. Eddaoudi, H. Li, O. M. Yaghi, *J. Am. Chem. Soc.* **2000**, *122*, 1391 – 1397.
[13] S. S. Y. Chui, S. M. F. Lo, J. P. H. Charmant, A. G. Orpen, I. D. Williams, *Science* **1999**, *283*, 1148 – 1150.
[14] A. C. Sudik, A. P. Côté, O. M. Yaghi, *Inorg. Chem.* **2005**, *44*, 2998 – 3000.
[15] M. Eddaoudi, J. Kim, N. Rosi, D. Vodak, J. Wachter, M. O'Keeffe, O. M. Yaghi, *Science* **2002**, *295*, 469 – 472.
[16] A. L. Spek, *J. Appl. Crystallogr.* **2003**, *36*, 7 – 13; A. L. Spek, PLATON, A Multipurpose Crystallographic Tool, Utrecht University, The Netherlands, **2006**; available via http://www.cryst.chem.uu.nl/platon (for Unix) and http://www.chem.gla.ac.uk/~louis/software/platon/ (for MS Windows).
[17] J. F. Byrne, H. Marsh in *Porosity in Carbons: Characterization and Applications* (Ed.: J. W. Patrick), Edward Arnold, London, **1995**, pp. 1 – 48; B. H. Davis, K. S. W. Sing in *Handbook of Porous Solids* (Eds.: F. Schüth, K. S. W. Sing, J. Weitkamp), Wiley-VCH, Weinheim, **2002**, Vol. 1, pp. 3 – 23.
[18] X. B. Zhao, B. Xiao, A. J. Fletcher, K. M. Thomas, *J. Phys. Chem. B* **2005**, *109*, 8880 – 8888; H. Tanaka, H. Kanoh, M. Yudasaka, S. Iijima, K. Kaneko, *J. Am. Chem. Soc.* **2005**, *127*, 7511 – 7516; R. Yaris, J. R. Sams, Jr., *J. Chem. Phys.* **1962**, *37*, 571 – 576; W. van Dingenen, A. van Itterbeek, *Physica* **1939**, *6*, 49 – 58.
[19] X. B. Zhao, S. Villar-Rodil, A. J. Fletcher, K. M. Thomas, *J. Phys. Chem. B* **2006**, *110*, 9947 – 9955.
[20] F. Stephanie-Victoire, A. M. Goulay, E. C. de Lara, *Langmuir* **1998**, *14*, 7255 – 7259.
[21] *Hydrogen, Fuel Cells & Infrastructure Technologies Program: Multi-Year Research, Development and Demonstration Plan*, U.S. Department of Energy, **2005**, http://www.eere.energy.gov/hydrogenandfuelcells/mypp/; *Basic Research Needs for the Hydrogen Economy*, report of the Basic Energy Sciences Workshop on Hydrogen Production, Storage, and Use, U.S. Department of Energy, **2004**, http://www.sc.doe.gov/bes/; E. Tzimas, C. Filiou, S. D. Peteves, J.-B. Veryret, *Hydrogen Storage: State-of-the-Art and Future Perspective*, European Commision, Institute for Energy, **2003**, http://ie.jrc.cec.eu.int/publications/scientific_publications/2003/P2003-181=EUR20995EN.pdf.

[22] *CRC Handbook of Chemistry and Physics*, 74th ed., CRC, Boca Ratan, **1993**.
[23] G. Férey, C. Mellot-Draznieks, C. Serre, F. Millange, J. Dutour, S. Surblé, I. Margiolaki, *Science* **2005**, *309*, 2040 – 2042; Correction: G. Férey, C. Mellot-Draznieks, C. Serre, F. Millange, J. Dutour, S. Surblé, I. Margiolaki, *Science* **2005**, *310*, 1119
[24] X. Zhao, B. Xiao, A. J. Fletcher, K. M. Thomas, D. Bradshaw, M. J. Rosseinsky, *Science* **2004**, *306*, 1012 – 1015; H. Chun, D. N. Dybtsev, H. Kim, K. Kim, *Chem. Eur. J.* **2005**, *11*, 3521 – 3529; B. Kesanli, Y. Cui, M. R. Smith, E. W. Bittner, B. C. Brockrath, W. Lin, *Angew. Chem.* **2005**, *117*, 74 – 77; *Angew. Chem. Int. Ed.* **2005**, *44*, 72 – 75.

